Published by Avanti Publishers

Journal of Chemical Engineering Research Updates

ISSN (online): 2409-983X

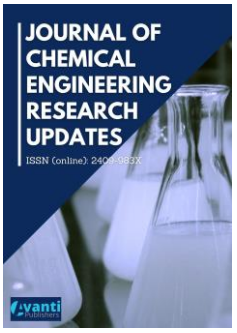

Behavior in Oxidation at 1000°C of Carbon-Containing Equimolar CoNiFeMnCr Alloys Added with Hafnium or Tantalum with High Contents

Patrice Berthod*

Institut Jean Lamour, Université de Lorraine, 2 allée André Guinier, Campus ARTEM, 54000 Nancy, France

ARTICLE INFO

Article Type: Research Article

Keywords:
HfC
TaC
Oxidation
High temperature
Equimolar HEA alloys

Timeline:
Received: November 29, 2022
Accepted: December 30, 2022
Published: December 31, 2022

Citation: Berthod P. Behavior in oxidation at 1000°C of carbon-containing equimolar CoNiFeMnCr alloys added with hafnium or tantalum with high contents. J Chem Eng Res Updates. 2022; 9: 60-71.

DOI: https://doi.org/10.15377/2409-983X.2022.09.7

ABSTRACT

In this work, HfC–and TaC–reinforced cast versions of the equimolar CoNiFeMnCr alloy (Cantor) were tested in oxidation at 1000°C in laboratory air. Chromium seemingly shared, with manganese, its role as a selectively oxidized element. The principal oxide to form externally was an M_2O_3 one in which Mn and Cr were present in various proportions depending on the proximity with the alloy's surface. The HfC carbides close to the oxidation front were oxidized in situ in HfO_2, with the release of carbon diffusing inwards after that and inducing the solid-state precipitation of blocky or acicular chromium carbides. The behavior of the TaC carbides present close to the oxidation front was different since they dissolved, and Ta diffused towards the oxidation front to form $CrTaO_4$ oxides. Even after 50 hours at 1000°C, the subsurfaces were more or less deeply impoverished in Cr and Mn, with minimal contents meager, especially for Mn. The evaluation of the Cr and Mn quantities and the exploitation of results in terms of equivalent oxide thickness and kinetic oxidation constant demonstrates that the resistance of the alloys against oxidation is feeble and must be significantly improved to allow benefiting of the superior high-temperature mechanical resistances of such alloys in practical application. For that, some ways are proposed.

*Corresponding Author
Email: patrice.berthod@univ-lorraine.fr
Tel: +(33) 3 72 74 27 29

1. Introduction

Recently, a new class of metallic materials has attracted high interest: the "high entropy alloys" (HEA). By mixing a series of different metals present in similar atomic quantities, disordered austenitic crystalline networks are obtained and are at the origin of interesting properties, notably mechanical. The most common HEAs involve cobalt, nickel, iron, and chromium, with the possible additional presence of aluminum [1], titanium [2], copper, and even silver [3]. A frequently met system involves manganese [4], and one of the earliest HEAs to appear was the Cantor alloy, the equimolar CoNiFeMnCr quinary alloy [5]. Beyond conventional casting, this alloy can be synthesized following other elaboration ways such as single–crystalline solidification [6] or additive manufacturing [7]. It is the subject of various investigations in the thermodynamic [8], mechanical [9], or diffusion [10] fields. Its mechanical behavior is of high level for temperatures not too high, but using it at 1000°C and beyond supposes that hard particles reinforce the grain boundaries of its polycrystalline versions to delay the intergrain decohesion (leading to the third stage of creep followed by rupture, for instance). Particularly efficient particles to strengthen polycrystalline superalloys for service temperatures of 1000°C and higher are monocarbides precipitating during final eutectic solidification. The script–like morphology of eutectic TaC and HfC favors the cohesion of neighbor grains and dendrites and allows extended–lasting use before failure [11-13].

The addition of carbon (0.5 wt.%) and Ta and Hf with high contents (7.4 wt.%, rated to respect the molar equivalence with the 0.5wt.%C) was tested recently to promote the formation of a dense interdendritic network of carbides, exclusively of the MC type to optimize the strengthening effect on alloys [14, 15]. Dense precipitations of HfC or TaC interdendritic carbides were successfully obtained. Consequently, an efficient reinforcement of the alloys against creep at elevated temperature with these carbides, which are closely imbricated with matrix and morphologically very stable even at elevated temperature. Investigations about the high-temperature properties of these alloys must be pushed further now, notably with exposures to hot air aiming to verify whether the oxidation resistance of these alloys, rich in Hf or Ta, which are elements very easy to oxidize, is high enough to do not threaten their sustainability during work in high-temperature gaseous mixtures. This is precisely the purpose of the present work.

2. Materials and Methods

The alloys with the same chemical compositions were fabricated, both with an equimolar CoNiFeMnCr base added with 0.5 wt.%C, and one with 7.44 wt.%Hf (alloy named “HFhea”) and the other with 7.44 wt.%Ta (named “TAhea"). They were elaborated using pure elements (ALFA AESAR, purity > 99.9 wt.%) available as small metallic slugs, flakes, and graphite rods. They were melted together in the water–cooled cold crucible of a high-frequency induction furnace (CELES, France) with 110kHz and 5kV operating parameters. The atmosphere in the melting chamber was made of 300 millibars of pure argon.

The obtained ingots, with a weight almost equal to 40 grams, were embedded in a cold resin mixture to facilitate their handling for the cutting steps of the sample preparation. Cutting was carried out using a metallographic saw. The obtained samples were of different types for each of the two alloys:

- apart to embed in resin (ESCIL, France), to grind (SiC papers from #240 to #1200 underwater as lubricant/coolant), and to polish (1µm alumina particles sprayed on textile disk, special lubricant) until the obtention of a mirror-like state: for microstructure control
- a parallelepipedic part (about 7mm '7mm '3mm) to grind all around with #1200 SiC paper: for the oxidation test

The microstructure control was done using a Scanning Electron Microscope JEOL JSM–2010LA (Japan), under an acceleration voltage of 15 to 20kV, in Back Scattered Electrons mode (SEM/BSE) for imaging (at several magnifications), and with Energy Dispersion Spectrometry (EDS) full frame and spot analysis (chemical composition of the alloy and all current phases).

The oxidation tests were carried out using a muffle resistive furnace (NABERTHERM). The samples were placed on a refractory ceramic piece which was itself placed in the hottest zone of the furnace. The alloys were oxidized

for 50 hours at 1000°C (atmosphere: laboratory air). At the end of the experiment, the furnace was switched off and left closed. It was opened only after complete cooling (room temperature). The ceramic with the oxidized samples were then taken out of the furnace. These were carefully handled and submitted to X–Ray Diffraction (XRD, D8Advance, Brüker, Cu K_α radiation). They were after that immersed in a liquid cold resin mixture which rigidified by preserving the oxides formed on the surfaces of the samples. After cross–sectional cutting (metallographic saw), grinding, and polishing (same procedure as the parts for initial microstructure control), the oxidized samples were examined (oxides, subsurface, bulk) using the SEM, in BSE mode and with EDS analysis (spot, profiles, elemental mapping).

3. Results and Discussion

3.1. Microstructure and Chemical Composition Control

The two alloys were successfully obtained by melting and solidification (Fig. **1**). After metallographic preparation of the two samples devoted to the microstructure and chemical controls, these were examined (SEM/BSE) and analyzed (EDS). Micrographs taken at low and high magnifications illustrate them as–cast state microstructures (Fig. **2** for the “HFhea” alloy, Fig. **3** for the “TAhea” alloy), which comply with the earlier observed microstructures [14, 15].

Both alloys are double–phased. They are made of a dendritic matrix and MC carbides. The matrix of the HFhea alloy is a chemically homogeneous solid solution of Co, Ni, Fe, Mn, and Cr, in which Hf is absent. The matrix of the TAhea alloy is also a homogeneous solid solution of Co, Ni, Fe, Mn, and Cr, but it additionally contains a part of tantalum. The second phase, HfC or TaC carbide, is of two types. They are pre–eutectic HfC (mainly gathered in clusters) and eutectic HfC (script–like shaped) for the HFhea alloy. The TAhea alloy also contains compact pre–eutectic carbides and script–like eutectic carbides, but the former is less numerous than the pre–eutectic HfC in the HFhea alloy. No pre–eutectic TaC formed clusters, and all stayed isolated.

The chemical compositions were controlled using EDS (full frame analyses). The results, displayed in Table **1**, allow checking that the wished contents were successfully obtained. Some spot analyses were additionally performed in the core of dendrites, and results showed that hafnium is absent in the matrix of the "HFhea" alloy (consequently, Hf is wholly involved in the HfC formation) while 2 wt.%Ta is present in the “TAhea” matrix.

X-maps acquired in the cores of the two alloys are presented in Fig. (**4**) and Fig. (**5**) for the “HFhea" alloy and the ”TAhea" one, respectively. It is visible that, in both cases, the matrix is chemically homogeneous concerning the Co, Ni, Fe, and Cr elements, but not for Mn.

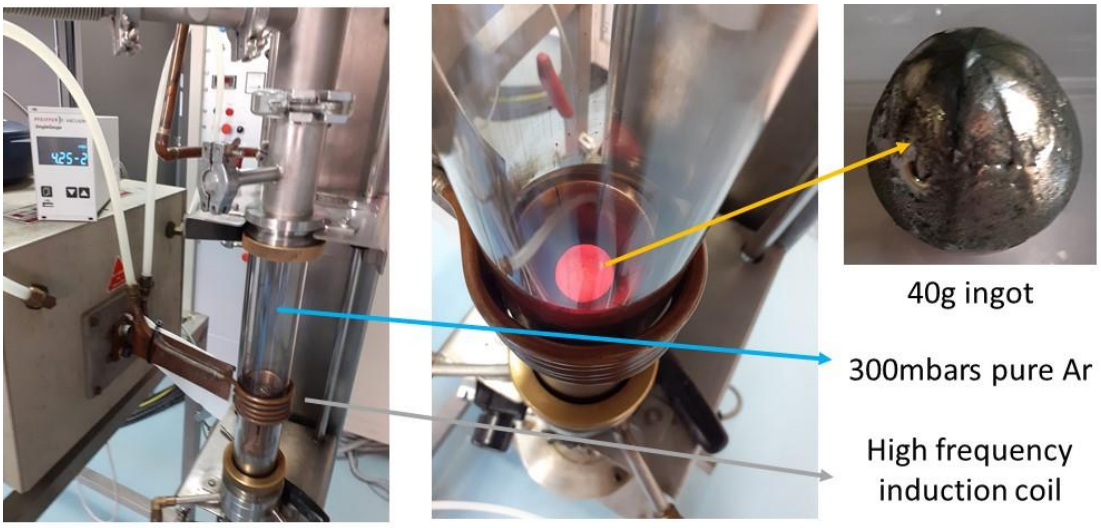

Figure 1: The apparatus used for alloy synthesis, solid-state cooling of a solidified ingot, and macrograph of the obtained ingot after complete cooling and extraction from the crucible.

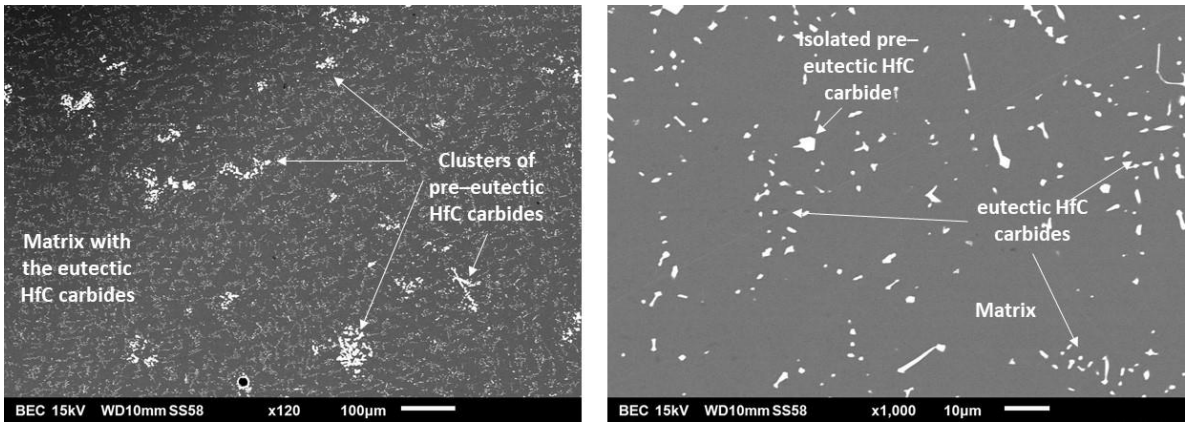

Figure 2: Low (left) and high (right) magnification SEM/BSE pictures illustrating the as–cast microstructure of the "HFhea" alloy.

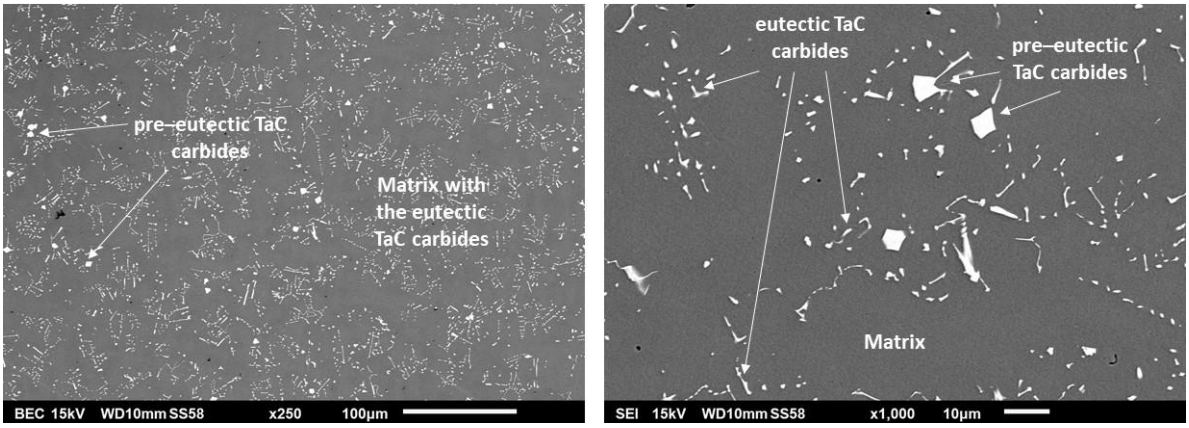

Figure 3: Low (left) and high (right) magnification SEM/BSE pictures illustrating the as–cast microstructure of the "TAhea" alloy.

Table 1: Chemical compositions of the two obtained alloys (average and standard deviation values calculated from the complete frame analyses on five ×250 areas).

Wt.%	Co	Ni	Fe	Mn	Cr	Hf or Ta
"HFhea" alloy (0.5 Wt.% C)	19.0 ±0.5	20.0 ±0.5	18.0 ±0.5	17.0 ±0.5	19.0 ±0.5	7.0 ±1.0
"Thea" alloy (0.5 Wt.% C)	18.5 ±0.5	20.0 ±0.5	18.0 ±0.5	18.0 ±0.5	19.0 ±0.5	6.3 ±1.0

Manganese has seemingly segregated in the last liquid zones to solidify (high concentration in the interdendritic spaces in each alloy). Hf and Ta are logically concentrated in the pre–eutectic and eutectic carbides, but Ta also seems to be weakly but homogeneously present in the matrix of the "TAhea" alloy. This is consistent with the EDS spot analysis results.

3.2. High-Temperature Oxidation Results

The samples devoted to the oxidation test were placed in the furnace, where they stayed for 50 hours. After complete cooling down to room temperature, the furnace was opened, and the oxidized samples were exited (Fig. **6**). Unfortunately, a part of the external oxides had spalled off during cooling (despite that this one was very slow). This can be a critical point in the case of thermal cycling at a much high temperature variation rate.

XRD was run on the oxidized samples. The obtained diffractograms (Fig. **7**) were challenging to exploit because of the presence of a relatively great number of oxides and the expected variations in the contents of the several

metals possibly present in each type of oxide. Besides the peaks corresponding to the alloys themselves (diffraction of some surface parts denuded by locally particularly intensive spallation of the external oxides), many diffraction peaks can be attributed to M_2O_3 and M_3O_4 oxides, with M representing Cr, Mn, or these two elements together (simultaneously present same oxides). One must also mention peaks corresponding to hafnium oxide (case of the HFhea alloy) or mixed oxide of chromium and tantalum (Thea alloy), more ($CrTaO_4$) or less (HfO_2) discrete but present.

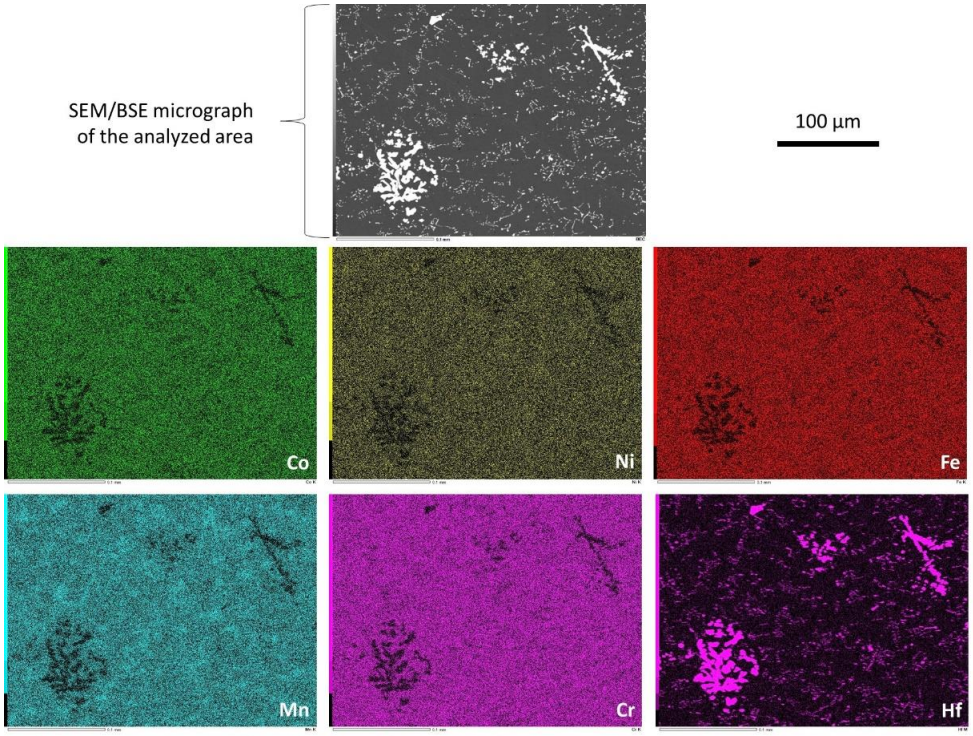

Figure 4: EDS elemental repartition maps in the "HFhea" alloy's microstructure.

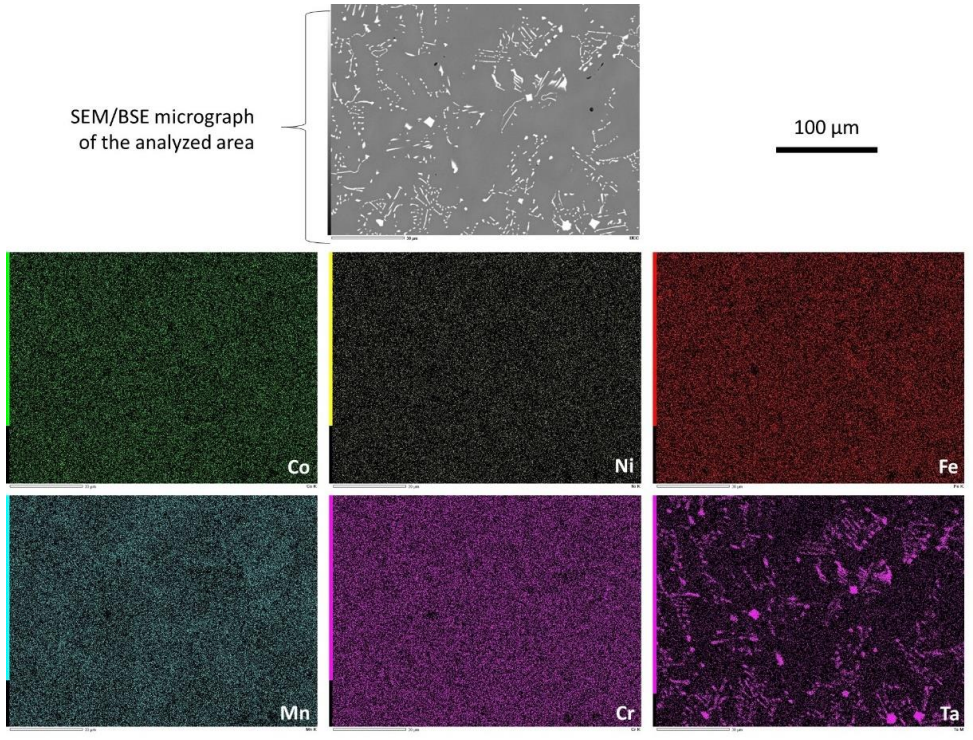

Figure 5: EDS elemental repartition maps in the "TAhea" alloy's microstructure.

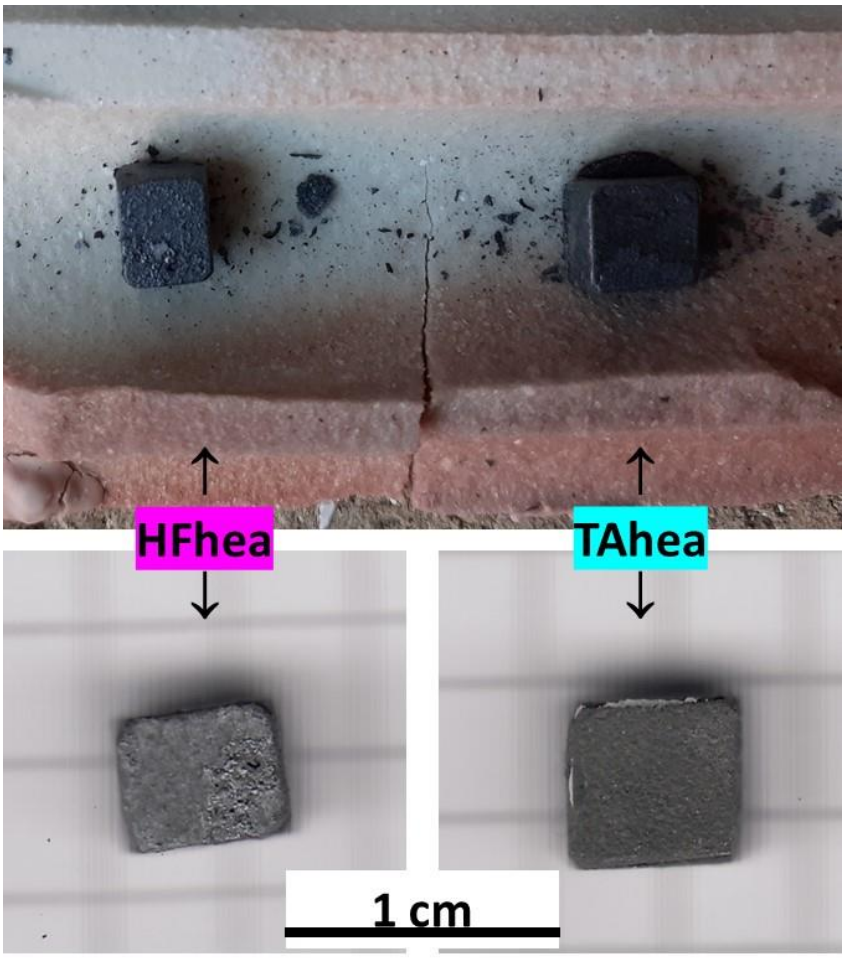

Figure 6: Macro photographs of the oxidized samples after their extraction outside the furnace and before their cross–sectional preparation.

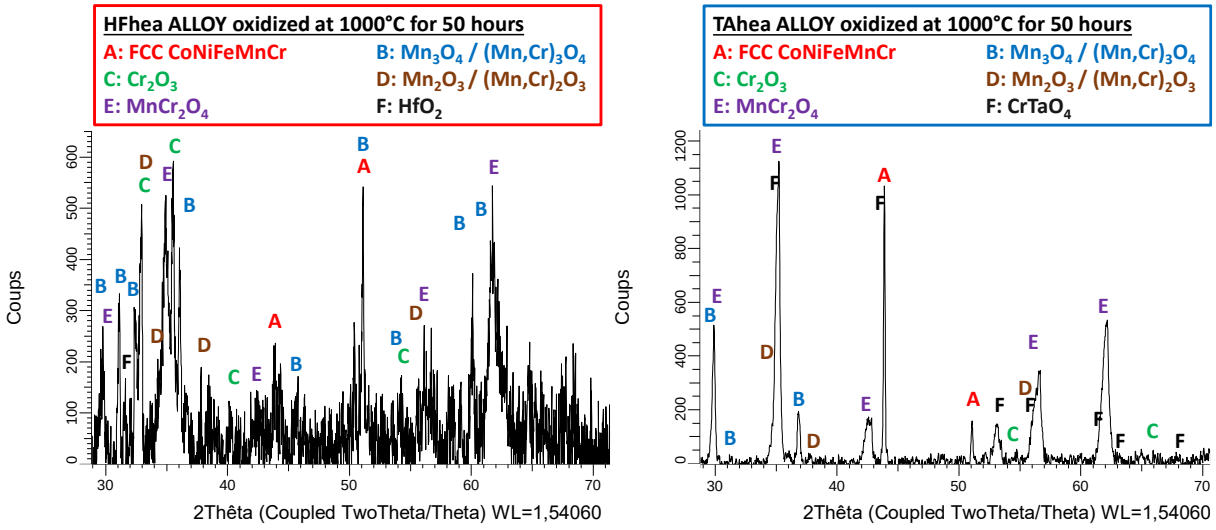

Figure 7: XRD diffractograms acquired on the oxidized surfaces of the two alloys (HFhea: left, TAhea: right).

After cross–sectional metallographic preparation, the external oxides and deteriorated subsurface were observed with the SEM in BSE mode at various magnifications and subjected to X–maps acquisition (Fig. **8** and Fig. **9** for the "HFhea" alloy, Fig. **10** and Fig. **11** for the "TAhea" one).

The “HFhea” alloy was covered by an external oxide scale (oxides of the M_2O_3 type, according to a series of EDS spot analyses), resulting from chromium and manganese oxidation. Chromium is more present in the part of this scale closest to the alloy, while manganese is more present in the other part of the scale, farther from the alloy. Internal oxidation in a 100 µm–deep subsurface zone, with locally deep penetrations of oxidation, possibly interdendritic, resulting in oxides of Mn and Cr. In the same 100µm–thick subsurface stripe (“A”–zone in Fig. **8**), the isolated HfC carbides and clusters of such carbides present close to the external surface were oxidized in situ. Carbides were converted in HfO_2 (appearing in bright gray, contrasting with the white HfC carbides). One can also notice the generalized precipitation of dark gray chromium carbides in a 200µm–thick, more internal band ("B"–zone in Fig. **8**). Such a curious phenomenon was earlier encountered in cobalt–based superalloys strengthened by tantalum carbides and chromium carbides [16], as well as in nickel–based ternary alloys containing chromium carbides [17]. In these earlier cases, the precipitation of chromium carbides in an inner zone of alloy still rich in Cr was explained by the inward diffusion of C following the dissolution of TaC and Cr_7C_3 carbides in more external zones under the effect of oxidation (carbides destabilization because of the Ta and Cr diffusion toward the oxidation front to be oxidized). In the present case, one can interpret this precipitation of chromium carbides by the inward diffusion of C released by the HfC carbides during their oxidation into HfO_2. In the present case too, C recombined deeper with a part of the chromium present in a solid solution in the matrix. The temperature and durations of the oxidation test carried out in this work are the same as the oxidation tests earlier applied to the alloys studied in these earlier works [16, 17] in which it was also noted that this phenomenon did not occur for the other oxidation tests of the same alloys performed at temperatures higher than 1100°C.

The oxidation features of the "TAhea” alloy (Fig. **10** and Fig. **11**) are more classical: no inward C diffusion is noted. Selective oxidation of Mn with Cr led to the external oxide of these two elements (oxides of the M_2O_3 type according to several EDS spot analyses, without real variation of the Mn and Cr proportions in the external scale). The one of Cr and Ta led to the formation of the same interfacial $CrTaO_4$ oxides as usually seen for alloys rich in Cr and Ta.

A common point can be found in the elemental X–maps between the two alloys: the inward development of Cr–depleted and Mn–depleted zones from the external surface. To get more quantitative information concerning these subsurface impoverishments in Mn and Cr, several EDS concentration profiles were acquired per alloy across the subsurface. Some examples illustrating the obtained profiles are given in Fig. (**12**). They evidence a decrease in the Cr and Mn content from a starting depth to the interface between the alloy and the external oxide scale. Table **2** gives the minimal values of these Cr and Mn contents.

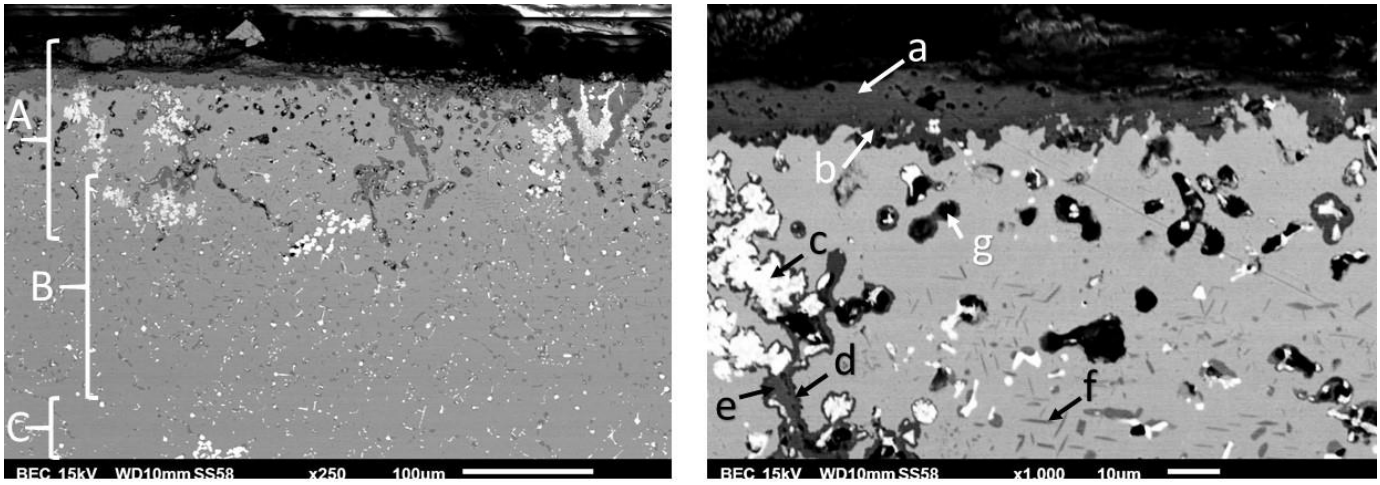

Figure 8: Low magnification (left) and high magnification (right) SEM/BSE cross–sectional pictures of the surface and subsurface of the “HFhea” alloy after 50 hours of oxidation at 1000°C; *A: external and internal oxidation, B: zone of chromium carbides sold state precipitation, C: part of an alloy not affected by oxidation; a and d: Mn–rich {Cr, Mn}–oxide, b and e: Cr–rich {Cr, Mn}–oxide, c: HfO_2 oxide, f: chromium carbides precipitated in a solid state during oxidation, g: hole due to oxidation.*

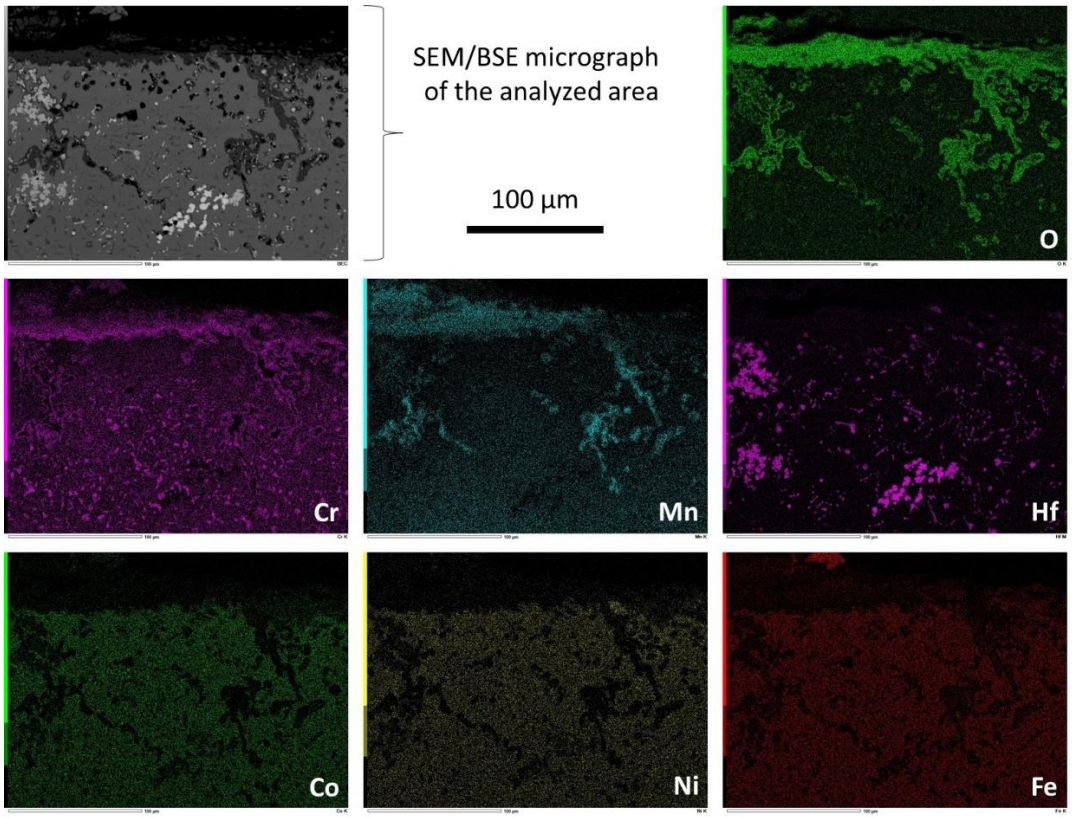

Figure 9: EDS elemental repartition maps in the surface and subsurface of the oxidized "HFhea" alloy.

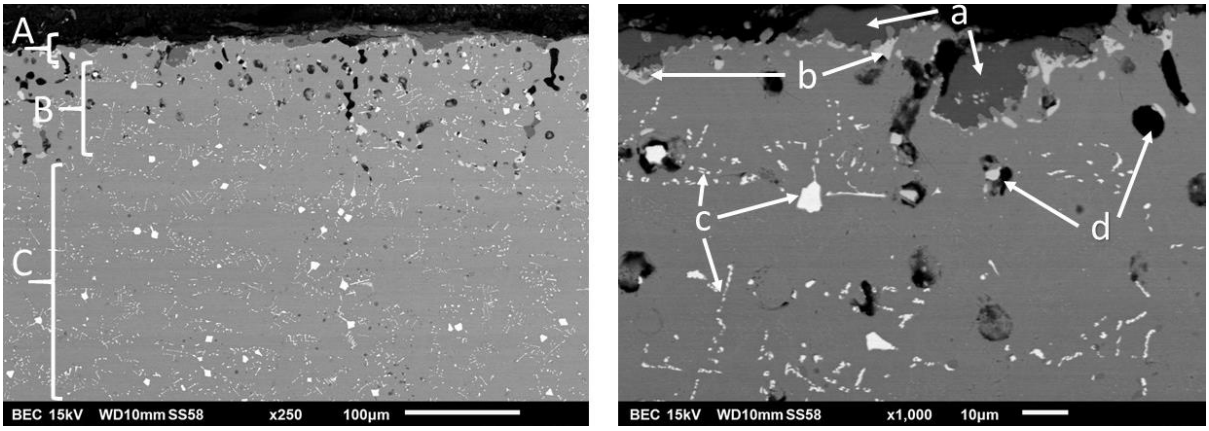

Figure 10: Low magnification (left) and high magnification (right) SEM/BSE cross–sectional pictures of the surface and subsurface of the "TAhea" alloy after 50 hours of oxidation at 1000°C; *A: external and internal oxidation, B: internal depth indirectly affected by oxidation, C: part of alloy not affected by oxidation; a: {Cr, Mn}–oxide, b: $CrTaO_4$ oxide, c: pre–eutectic and eutectic (fragmented) TaC carbides, d: voids due to oxidation.*

Table 2: The values of some parameters characterizing the Cr and Mn variations in the subsurfaces of the two alloys affected by oxidation.

Oxidized Alloys	Cr min (Wt.%)	Cr–Depleted Depth (µm)	Mn min (Wt.%)	Mn–Depleted depth (µm)
"HFhea" alloy	10.2 ±3.7	200 – 360	2.1 ±0.7	120–180
"Thea" alloy	15.8 ±0.3	36 – 44	1.2 ±0.2	61 – 82

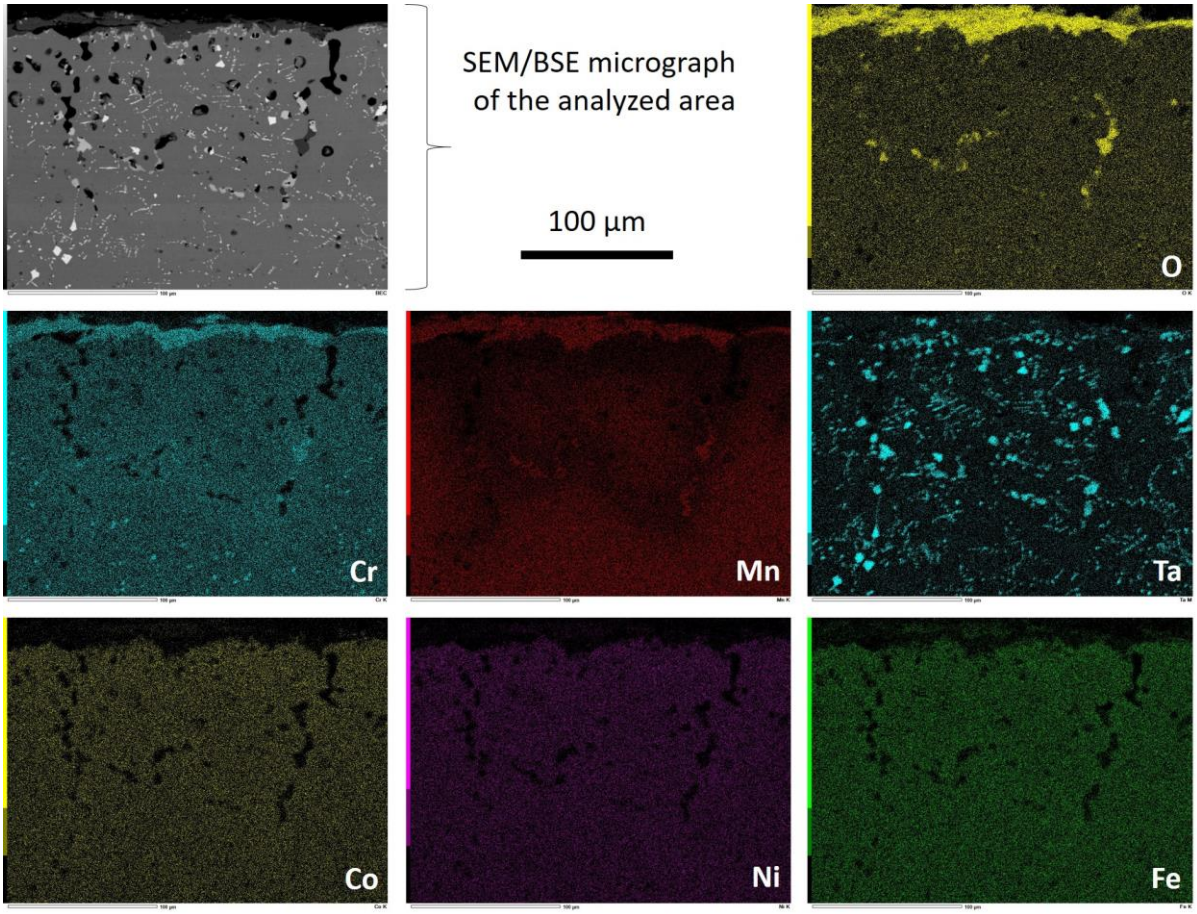

Figure 11: EDS elemental repartition maps in the surface and subsurface of the oxidized "TAhea" alloy.

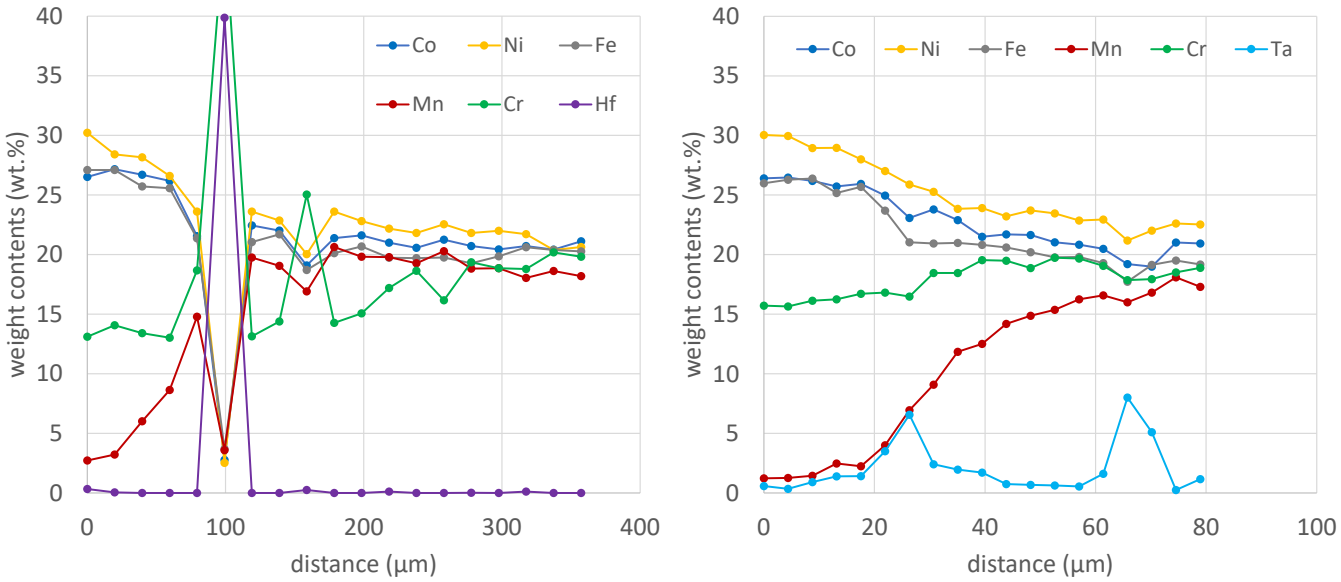

Figure 12: Concentrations profiles acquired from the oxide scale/alloy interface across the subsurface affected by oxidation (left: "HFhea" alloy, right "TAhea" alloy).

About 10 wt.%Cr remain in the extreme surface for the "HFhea" alloy, while the value is five points higher for the "TAhea" alloy. In both cases, the Cr content is lower than what is usually considered for cobalt and nickel alloys to behave longer as chromia–forming alloys at high temperatures. Indeed the threshold is 30 wt.%Cr for cobalt

alloys (i.e., already higher than the initial Cr contents of the present alloys) and 20 wt.% for Ni alloys (i.e., their initial Cr contents). For such criterion inherited from Cr–rich superalloys, both alloys seem to be next to catastrophic oxidation, especially the "HFhea" alloy. In the present case, manganese seems to play an important role in oxidation. As chromium, most of the manganese in the subsurface diffused to the oxidation front, and the greatest part of the oxides formed is composed of complex oxide involving Mn and Cr together.

Furthermore, the Mn contents in alloy close to the interface with the external oxide scale are much lower than the Cr contents. Measuring the depth of Cr–depleted and Mn–depleted zones (Table **2**, too) evidences that, between the two alloys, the one which lost the greatest quantities of chromium and manganese is seemingly the "HFhea" alloy. To verify this information quantitatively, balance sheets in Cr and Mn lost by each alloy per surface unit area were obtained by exploiting two profiles per alloy according to what was previously done for chromium in the subsurface of a Ni – 30Cr alloy after oxidation at various temperatures ranging from 1000 to 1300°C [18]. One can remind the successive calculations steps with the following formula:

$$\frac{m_X}{S} = \rho_{alloy} \times \int_0^{Ddepth_X} [f_w^X - f_w^X(x)] \times dx \qquad (E1)$$

for specifying the mass of the X element (X = Cr or Mn) lost per surface unit area $\frac{m_X}{S}$, with ρ_{alloy}, $Ddepth_X$, f_w^X, and $f_w^X(x)$ being the volume mass of the alloys (7.9g/cm^3), the X–depletion depth (Table **2**), the weight content in X in the alloy and the weight content in X at the depth x from the external alloy surface, respectively);

$$\frac{n_X}{S} = \left[\frac{\frac{m_X}{S}}{M_X}\right] \qquad (E2)$$

for specifying the number of moles of X (X = Cr or Mn) lost by the alloy per surface unit area ($\frac{n_X}{S}$), with M_X being the molar mass of X (55 g/Mol for Mn, 56g/Mol for Cr);

$$\frac{n_{(Mn,Cr)_2O_3}}{S} = \frac{1}{2} \times \left(\frac{n_{Cr}}{S} + \frac{n_{Mn}}{S}\right) \qquad (E3)$$

$$e_{(Mn,Cr)_2O_3} = \frac{\frac{n_{(Mn,Cr)_2O_3} \times (2 \times (M_{Cr} + M_{Mn}) / 2 + 3 \times M_O)}{S}}{\rho_{(Mn,Cr)_2O_3}} \qquad (E4)$$

for specifying the number of moles of $(Cr,Mn)_2O_3$ oxides formed per surface unit area $\frac{n_{(Mn,Cr)_2O_3}}{S}$, and the corresponding thickness of this oxide $e_{(Mn,Cr)_2O_3}$ ($with\ \rho_{(Mn,Cr)_2O_3}$= 4.86g/cm^3 for the volume mass of the oxide;

$$Kp = \frac{1}{2} \times \frac{\left(\frac{3}{2} \times \left(\frac{n_{Cr}}{S} + \frac{n_{Mn}}{S}\right) \times M_O\right)^2}{Timox} \quad) \qquad (E5)$$

for specifying the value of the kinetic parabolic constant Kp, with M_O=16g/Mol and $Timox$ = 50h = 180,000s.

This led to the quantities of Cr, and Mn lost per cm² displayed in Table **3**. These results demonstrate that much more Cr and Mn have quitted the "HFhea" alloy to be oxidized, compared with the "TAhea" one. Furthermore, by converting these Cr and Mn masses per cm^2 of a surface into moles numbers, the numbers of moles of M_2O_3 oxides were deduced and converted in mass per cm^2 and finally in equivalent oxide thickness using an average value of the density (between the chromia density and the Mn_2O_3 one). These values of equivalent thickness and the values of parabolic constant Kp to which they lead are presented in Table **3** again. This allows realizing that both alloys oxidized considerably faster than the reference Ni–30Cr at the same temperature (about 35 and 250' 10^{-12} g^2 cm^{-4} s^{-1} for "TAhea" and "HFhea" respectively, against only 2.8' 10^{-12} g^2 cm^{-4} s^{-1} for the Ni–30Cr [18]). With equivalent Kp values between ten times and one hundred times higher than for a the chromia–forming Ni–30Cr alloy, the resistance of these two alloys can be considered poor and insufficient for high-temperature uses in hot air or a mixture of oxidant gases.

Table 3: Quantification of the masses of chromium and manganese lost by the alloys, of the corresponding equivalent thicknesses of M_2O_3 oxide scale and parabolic constant values.

Oxidized Alloys	Lost Cr (mg/cm^2)	Lost Mn (mg/cm^2)	$(Cr, Mn)_2O_3$ Thickness (µm)	Kp Constant ('10^{-12} g^2 cm^{-4} s^{-1})
"HFhea" alloy	8 – 10	8 – 16	51 – 76	166 – 362
"Thea" alloy	0 – 1	5 – 8	17 – 25	30 – 37

4. Conclusion

The two alloys studied in this work can be described as composite materials combining a CoNiFeMnCr equimolar matrix and an MC carbide network. They look like very promising materials in the mechanical field since their principle cumulates the advantages of a HEA alloy (intrinsically strong matrix) and of a dense interdendritic network made of eutectic HfC or TaC carbides. These ones are known for their script–like shape, very favorable to creep resistance and their high morphological stability at elevated temperatures leading to the long sustainability of their strengthening effect. The first results of high-temperature creep tests performed in an inert atmosphere demonstrate the interest of such association for the mechanical resistance at high temperatures of alloys of this type [19].

Unfortunately, according to the present study, it is evident that the behavior in high-temperature oxidation needs to be more satisfactory. Due to the massive participation of manganese in the oxidation process, hindering the action of chromium, many oxides form with outward and inward growth. Oxidation is rapid – much faster than a model Ni–30Cr alloy – since the usual chromia scale develops in only a limited manner (not homogenously present inner layer), and the diffusion of the species involved in the oxidation process is much less slowed down as in chromia–forming alloys. Irregularly inward-grown oxides and more or less deep local oxide penetrations were noticed: this should threaten the mechanical resistance of such alloys in case of use in hot oxidant atmospheres.

Significant improvement in oxidation behavior is thus achieved before thinking about using such alloys for practical applications. Giving a more critical role to chromium at the expense of manganese is a way to explore. Alloys based on nonequimolar $CoNiFeMnCr_{1.5}$ or $CoNiFeMnCr_2$ HEAs reinforced by HfC or TaC may represent a potentially interesting way. This will be tested soon. Protective coating deposition is also another possibility to consider.

References

[1] Dabrowa J, Kucza W, Cieslak G, Kulik T, Danielewski M, Yeh JW. Interdiffusion in the FCC-structured Al-Co-Cr-Fe-Ni high entropy alloys: experimental studies and numerical simulations. J Alloys Compd. 2016; 674: 455-62. https://doi.org/10.1016/j.jallcom.2016.03.046

[2] Stepanov ND, Shaysultanov DG, Tikhonovsky MA, Zherebtsov SV. Structure and high-temperature mechanical properties of novel non-equiatomic Fe-(Co,Mn)-Cr-Ni-Al-(Ti) high entropy alloys. Intermetallics. 2018; 102: 140-51. https://doi.org/10.1016/j.intermet.2018.09.010

[3] Nagase T, Todai M, Nakano T. Liquid phase separation in Ag-Co-Cr-Fe-Mn-Ni, Co Cr-Cu-Fe-Mn-Ni and Co-Cr-Cu-Fe-Mn-Ni-B high entropy alloys for biomedical application. Crystals. 2020; 10(6): 527. https://doi.org/10.3390/cryst10060527

[4] Bracq G, Laurent-Brocq M, Perriere L, Pires R, Joubert JM, Guillot I. The Fcc solid solution stability in the Co-Cr-Fe-Mn-Ni multi-component system. Acta Met. 2017; 128: 327-36. https://doi.org/10.1016/j.actamat.2017.02.017

[5] Choi WM, Jung S, Jo YH, Lee S, Lee BJ. Design of new face-centered cubic high entropy alloys by thermodynamic calculation. Met Mater Int. 2017; 23(5): 839-47. https://doi.org/10.1007/s12540-017-6701-1

[6] Kawamura M, Asakura M, Okamoto NL, Kishida K, Inui H, George EP. Plastic deformation of single crystals of the equiatomic Cr-Mn-Fe-Co-Ni high-entropy alloy in tension and compression from 10 K to 1273 K. Acta Mater. 2021; 203: 116454. https://doi.org/10.1016/j.actamat.2020.10.073

[7] Haase C, Tang F, Wilms MB, Weisheit A, Hallstedt B. Combining thermodynamic modeling and 3D printing of elemental powder blends for high-throughput investigation of high-entropy alloys - towards rapid alloy screening and design. Mater Sci Eng. A 2017; 688: 180-9. https://doi.org/10.1016/j.msea.2017.01.099

[8] Song H, Ma Q, Zhang W, Tian F. Effects of vacancy on the thermodynamic properties of Co-Cr-Fe-Mn-Ni high-entropy alloys. J Alloys Compd. 2021; 885: 160944. https://doi.org/10.1016/j.jallcom.2021.160944

[9] Shafiei A. Simple approach to model the strength of solid-solution high entropy alloys in Co-Cr-Fe-Mn-Ni system. Condens Matter. 2020; 1-28. arxiv logo>cond-mat>arXiv:2005.07948

[10] Kucza W, Dabrowa J, Cieslak G, Berent K, Kulik T, Danielewski M. Studies of "sluggish diffusion" effect in Co-Cr-Fe-Mn-Ni, Co-Cr-Fe-Ni and Co-Fe-Mn-Ni high entropy alloys; determination of tracer diffusivities by combinatorial approach. J Alloys Compd. 2018; 731: 920-8. https://doi.org/10.1016/j.jallcom.2017.10.108

[11] Berthod P, Conrath E. Mechanical and chemical properties at high temperature of {M-25Cr}-based alloys containing hafnium carbides (M=Co, Ni or Fe): creep behavior and oxidation at 1200°C. J Mater Sci Technol Res. 2014; 1: 7-14. DOI:10.15377/2410-4701.2014.01.01.2

[12] Michon S, Aranda L, Berthod P, Steinmetz P. High temperature evolution of the microstructure of a cast cobalt base superalloy. Consequences on its thermomechanical properties. Metall Res Technol. 2004; 9: 651-62. https://doi.org/10.1051/metal:2004116

[13] Berthod P, Conrath E. Creep and oxidation kinetics at 1100 °C of nickel-base alloys reinforced by hafnium carbides. Mater Des. 2016; 104: 27-36. https://doi.org/10.1016/j.matdes.2016.04.079

[14] Berthod P. As-cast microstructures of high entropy alloys designed to be TaC-strengthened. J Met Material Res. 2022; 5(2): 1-10. https://doi.org/10.30564/jmmr.v5i2.4685

[15] Berthod P. As–cast microstructures of HEA designed to be strengthened by HfC. J Eng Sci Innov. 2022; 7(3): 305-14. https://jesi.astr.ro/wp-content/uploads/2022/10/3_Patrice-Berthod.pdf

[16] Berthod P, Michon S, Di Martino J, Mathieu S, Noël S, Podor R, Rapin C. Thermodynamic calculations for studying high temperature oxidation of superalloys. Calphad. 2003; 27: 279-88. https://doi.org/10.1016/j.calphad.2003.12.002

[17] Berthod P. Experimental and thermodynamic study of nickel-based alloys containing chromium carbides, Part II: study of the sub-surface characteristics of Ni–30wt%Cr–xC alloys oxidized at high temperature using thermodynamic calculations. Calphad. 2008; 32: 492-9. https://doi.org/10.1016/j.calphad.2008.06.005

[18] Berthod P. Kinetics of high temperature oxidation and chromia volatilization for a binary Ni–Cr alloy. Oxid Met. 2005; 64(3/4): 235-52. https://doi.org/10.1007/s11085-005-6562-8

[19] Berthod P. Strengthening against creep at elevated temperature of HEA alloys of the CoNiFeMnCr type using MC-carbides. In: Proceedings to the TMS 2023 Annual Meeting & Exhibition, San Diego: 2023.